World Scientific
www.worldscientific.com

Theoretical study of excitation profiles of coherent anti-stokes Raman Scattering (CARS) and applications to carotenoids

G. D. Tatishvili [ID]*, M. G. Zakaraya [ID]† and D. G. Gogoli [ID]‡

*R. Agladze Institute of Inorganic Chemistry and Electrochemistry,
I. Javakhishvili Tbilisi State University,
11 Elizbar Mindeli St., 0186 Tbilisi, Georgia*
*tati@iise.ge
†merzakaraya@gmail.com
‡davit.gogoli@tsu.ge

S. P. Kruchinin [ID]

*Bogolyubov Institute for Theoretical Physics,
National Academy of Sciences of Ukraine,
14-b Metrolohichna St., 03143 Kyiv, Ukraine*
sergeikruchinin@yahoo.com

Coherent anti-Stokes Raman Scattering (CARS) spectroscopy is a nonlinear optical technique that is used to investigate many different chemical and biological systems. This tool is very efficient and essentially completely rejects fluorescence. As is well known, the excitation profiles of resonance CARS are mostly used to estimate the origin shift parameters with electronic excitation for vibrations with resonantly enhanced Raman components that give information about the molecular structure and its changes in an excited electronic state. Certainly, it is necessary to have an appropriate theoretical model for pragmatically representing these processes and considering the joint (simultaneous) impact of different broadening mechanisms. The theoretical model presented in the paper is the most general and is free from *a priori* assumptions. Also, the mathematical algorithm created on its basis is flexible and fast for quantitative calculations.

Keywords: CARS spectroscopy; vibronic interactions; β-carotene.

1. Theoretical Part

In the Coherent anti-Stokes Raman Scattering (CARS) process, three waves, two at the pumping frequency ω_1 and one at the Stokes frequency ω_2, interact with a target

---

*Corresponding author.

molecule. Nonlinear optical effects caused by the third-order nonlinear susceptibility $\chi^{(3)}$ mechanism leads to the formation of new coherent radiation at the anti-Stokes frequency $\omega_3 = 2\omega_1 - \omega_2$. The efficiency of such a process attained in any medium grows sharply as difference $\Delta = \omega_1 - \omega_2$ approaches the frequency of the Raman active transition $\omega_{n_g} = E_{n_g}/\hbar$. In order to obtain the excitation profiles, one scans the frequencies ω_1 and ω_2 in such a way that $\Delta = \omega_1 - \omega_2 = E_{n_g}$ is satisfied all the time. The shape of excitation profiles is very sensitive to different broadening mechanisms: homogeneous and inhomogeneous.[1] Consequently, identification of the contributions from broadening mechanisms along with the determination of the parameters characterizing the change of the equilibrium geometry of molecules in the excited electronic state are very important. Therefore, the joint influence effects of condensed medium and intramolecular process on the excitation profiles of CARS spectral lines are studied.

The intensity distribution of the CARS spectral line within the framework of the basic model of the vibronic interaction theory has the form[1]

$$P_{(n_g)}(\omega_1) = \left| \chi^{(3)}_{(n_g)}(\omega_1) \equiv \sum_{k_e=0}^{\infty} \sum_{m_e=0}^{\infty} \chi^{k_e, m_e}_{n_g}(\omega_1) \right|^2, \tag{1}$$

where

$$\chi^{k_e, m_e}_{n_g} \cong \mu_{eg}^4 \frac{\langle O_g | m_e \rangle \langle m_e | n_g \rangle \langle n_g | k_e \rangle \langle k_e | O_g \rangle}{(\omega_1 - \omega_{eg} - E_{k_e} + i\Gamma_{k_e})(\Delta - E_{n_g} + \Gamma_{n_g})(\omega_3 - \omega_{eg} - E_{m_e} + i\Gamma_{m_e})}. \tag{2}$$

In Eq. (2), μ_{eg} is the electronic dipole moment of the transition, $|0_g\rangle$ and $|n_g\rangle|k_e\rangle$ are the vibrational wave functions of the vibrational ground and n_gth excited states in the electronic ground state, respectively; $|k_e\rangle$ and $|m_e\rangle$ are the corresponding wave functions in the excited electronic state; E_{k_e} and E_{m_g} are the vibrational energies of $|k_e\rangle$ and $|m_e\rangle$, respectively, counted from the purely electronic transition energy ω_{eg}; Γ_{k_e} and Γ_{m_e} are the decay constants of the vibronic states $k_e\rangle$ and $|m_e\rangle$, respectively.

According to Ref. 1 a Gaussian distribution is the most natural form of the function characterizing the variation in the magnitude of the gap ω_{eg} relative to the average value of this gap, $\bar{\omega}$, i.e.

$$\rho(\omega_{eg}) = (\sqrt{2\pi}\sigma)^{-1}\exp[-(\omega_{eg} - \bar{\omega}_{eg})^2/2\sigma^2], \tag{3}$$

where $\rho(\omega_{eg})$ is the probability that the gap assumes the particular value ω_{eg} and σ is the inhomogeneous width of the distribution. The correct averaging of $\chi^{(3)}$ over the distribution of Eq. (3) was first accomplished in Ref. 1; however, both to obtain the theoretical analysis of the final expressions and there use in quantitative computations are extremely difficult.

Having substituted $\Delta \equiv \omega_1 - \omega_2 \approx \varepsilon_{n_g}$ and transforming the remaining part of the denominator into the form

$$\frac{(\omega_1 - \omega_{eg} - \varepsilon_{k_e} + i\Gamma_{k_e})^{-1} - (\omega_3 - \omega_{eg} - \varepsilon_{m_e} + i\Gamma_{m_e})^{-1}}{(\omega_1 - \omega_{eg}) + (\varepsilon_{k_e} - \varepsilon_{m_e}) + i(\Gamma_{m_e} - \Gamma_{k_e})}, \tag{4}$$

it is not difficult to carry out the averaging of $\chi_{n_g}^{(3)}(\omega_1)$ with respect to Eq. (3) with consideration of

$$\langle\langle(\omega_1 - \omega_{eg} - \varepsilon + i\Gamma)^{-1}\rangle\rangle = -\frac{i}{\sigma}\sqrt{\frac{\pi}{2}}W\left(\frac{\omega_1 - \omega_{eg} - \varepsilon + i\Gamma}{\sqrt{2}\sigma}\right). \tag{5}$$

Here, $W(z)$ is a complex function[2]

$$W(z) = \frac{i}{\pi}\int_{-\infty}^{\infty}\frac{\exp(-t^2)dt}{z-t} = \exp(-z^2)\mathrm{erfc}(-iz) \quad (\mathrm{Im}z > 0), \tag{6}$$

connected by a simple relation with the plasma dispersion function

$$Z(\upsilon + i\xi) = i\sqrt{\pi}W(\upsilon + i\xi). \tag{7}$$

We separated the real Ψ and imaginary (φ) parts of the function $W(z = \upsilon + i\xi)$ from (6) for arbitrary values of ξ and υ in the form of rapidly converging series.[3] In the following we present simpler but still accurate expressions for the functions:

$$\psi(\upsilon;\xi) = \exp(-\upsilon^2)\left\{\exp(\xi^2)\cos(2\xi\upsilon)[1 - cth(2\pi\xi)]\right.$$

$$\left. + (2\xi/\pi)\sum_{n=-\infty}^{\infty}\exp(-n^2/4)ch(n\upsilon)/(n^2 + 4\xi^2)\right\} \tag{8}$$

and

$$\varphi(\upsilon;\xi) = \exp(-\upsilon^2)\left\{\exp(\xi^2)\sin(2\xi\upsilon)[cth(2\pi\xi) - 1]\right.$$

$$\left. + (1/\pi)\sum_{n=-\infty}^{\infty}n\exp(-n^2/4)sh(n\upsilon)\right/(n^2 + 4\xi^2)\right\}, \tag{9}$$

which were obtained with the aid of the summation

$$\left(\frac{2\xi}{\pi}\right)\sum_{n=-\infty}^{\infty}\exp\left(-\frac{n^2}{4}\right)(n^2 + 4\xi^2)^{-1} = \exp(\xi^2)[cth(2\pi\xi) - \mathrm{erf}(\xi)] \tag{10}$$

The function $\Psi(\upsilon;\xi)$ is known in spectroscopy as the *Voigt* profile[3]; it is the outcome of the convolution of the Lorentzian and Gaussian functions and determines the dependence of the different spectral coefficients on frequency (υ is the dimensionless detuning of the resonance frequency) and plays an important role in all questions of line-shape analyses.

It is not difficult to show that near the maximum ($|\upsilon| < 1$) (and more accurately the smaller fundamental parameter $\xi \equiv \Gamma/\sqrt{2}\sigma$). That is one may approximate $\Psi(\upsilon;\xi)$ with

$$\Psi(\upsilon;\xi) = \exp(-\upsilon^2)[a(\xi) - b(\xi)\cos(2\upsilon\xi)], \quad \xi|\upsilon| < 1, \tag{11}$$

with coefficients

$$a(\xi) = \frac{1}{\sqrt{\pi\xi}}, \quad b(\xi) = \exp(\xi^2)\mathrm{erfc}(\xi) - (\xi\sqrt{\pi})^{-1}, \tag{11'}$$

when the inhomogeneous (Gaussian) mechanism dominates the homogenous (Lorentzian). So far as the far wings of the Voigt curve are symmetrical with respect to $\upsilon = 0$, they approximate the shape of the Lorentzian line

$$\Psi(\upsilon;\xi) = \left[\frac{\xi}{\sqrt{\pi}}(\xi^2 + \upsilon^2)\right]\left[1 + \frac{\upsilon^2}{(\xi^2 + \upsilon^2)^2}\right], \quad \xi|\upsilon| > 1, \tag{12}$$

where the expression in the second set of brackets gives a correction to the Lorentzian line for the wing of a Voigt curve.

Finally, so far as returning to analyses of (1)–(3), it is easy to find the antisymmetric function $\varphi(-\upsilon;\xi) = -\varphi(\upsilon;\xi)^3$ which describes the dispersion curve. According to (7) and (8), by simple differentiation of $\varphi(\upsilon;\xi)$,

$$\varphi(\upsilon;\xi) = \frac{(2\xi)^{-1}\partial\Psi}{\partial\upsilon} + (\upsilon/\xi)\Psi(\upsilon;\xi). \tag{13}$$

Returning to the averaging of the expression for $\chi_{n_g}^{(3)}(\omega_1)$ over the distribution of (3), considering (2), (5), (8) and (9), we find it more complicated to write

$$
\begin{aligned}
\langle\chi_{n_g}^{k_e,m_e}(\omega_1)\rangle = {} & \frac{\mu_{eg}^4}{\Gamma_{n_g\sigma}}\sqrt{\frac{\pi}{2}}\frac{\langle O_g|m_e\rangle\langle m_e|n_g\rangle\langle n_g|k_e\rangle\langle k_e|O_g\rangle}{(E_{n_g} + E_{k_e} - E_{m_e})^2 + (\Gamma_{m_e} - \Gamma_{k_e})^2} \\
& \times \{(\Gamma_{m_e} - \Gamma_{k_e})[\varphi(\upsilon_{m_e};\xi_{m_e}) - \varphi(\upsilon_{k_e};\xi_{k_e})] \\
& - (E_{n_g} + E_{k_e} - E_{m_e})[\psi(\upsilon_{k_e};\xi_{k_e}) - \psi(\upsilon_{m_e};\xi_{m_e})] \\
& + i(\Gamma_{m_e} - \Gamma_{k_e})[\psi(\upsilon_{k_e};\xi_{k_e}) - \psi(\upsilon_{m_e};\xi_{m_e})] \\
& + i(E_{n_g} + E_{k_e} - E_{m_e})[\varphi(\upsilon_{m_e};\xi_{m_e}) - \varphi(\upsilon_{k_e};\xi_{k_e})]\}, \tag{14}
\end{aligned}
$$

where

$$\upsilon_{k_e} \equiv \frac{\omega_1 - \omega_{eg} - E_{k_e}}{\sqrt{2}\sigma}, \quad \upsilon_{m_e} \equiv \frac{\omega_1 - \bar{\omega}_{eg} - E_{m_e} - E_{n_g}}{\sqrt{2}\sigma}, \quad \xi_{k_e(m_e)} \equiv \frac{\Gamma_{k_e(m_e)}}{\sqrt{2}\sigma} \tag{14'}$$

and the functions $\psi(\upsilon;\xi)$ and $\varphi(\upsilon;\xi)$ are given by Eqs. (8) and (9).

According to Eq. (4), $\langle\chi^{(3)}\rangle$ is a complex quantity whose real and imaginary parts make significant contributions to the intensity distribution in CARS spectra and to the formation of the corresponding excitation profiles $p_{n_g}(\omega_1)$.

2. Numerical Analysis

For the validation of the developed theory, an analysis of experimental data of CARS excitation profiles[4,5] of trans-β-carotene dissolved in benzene at room temperature was carried out. Two strongly expressed peaks at $1527\,\mathrm{cm}^{-1}$ and $1158\,\mathrm{cm}^{-1}$ were observed in the CARS spectrum of trans-β-carotene belonging to the C=C and C–C stretching modes, respectively.

The mostly adopted approach to determining the numerical values of dimensionless equilibrium shifts $Q_{0j}(j = 1, \ldots, N)$, Γ, and σ implies determining the

parameters that show the best compliance theory and experiment. For a polyatomic molecule having several active vibrations, this is a time-consuming task that is equivalent to finding the minimum in multidimensional space for the following functional:

$$\delta = \sum_{i=1}^{p} [\langle \chi_{n_g}^{k_e,m_e}(\omega_i; Q_{0_1}, \ldots, Q_{0_N}; \xi; \sigma)\rangle - \chi_{n_g}(\omega_i)]^2, \tag{15}$$

where p is the number of experimental points ω_i on the frequency scale with the measured values of $\chi_{n_g}(\omega_1)$ at those points, and N is the number of active vibrational modes.

The minimization of the functional (15) by least squares method for the CARS excitation profiles for the two active modes with $\Omega_1 = 1527 \, \text{cm}^{-1}$ (C=C) and $\Omega_2 = 1158 \, \text{cm}^{-1}$ (C–C) can be done independently. It gives a good enough agreement with the experiment, but at the same time noticeable difference can be observed in the values of some main parameters. In particular,

$$Q_{0_1} = 1.3, \quad Q_{0_2} = 0.9, \quad \Gamma = 55 \, \text{cm}^{-1} \quad \text{and} \quad \sigma = 352 \, \text{cm}^{-1}, \tag{16}$$

for the CARS excitation profiles of the C=C stretching mode, and

$$Q_{0_1} = 0.3, \quad Q_{0_2} = 0.9, \quad \Gamma = 58 \, \text{cm}^{-1} \quad \text{and} \quad \sigma = 391 \, \text{cm}^{-1}, \tag{17}$$

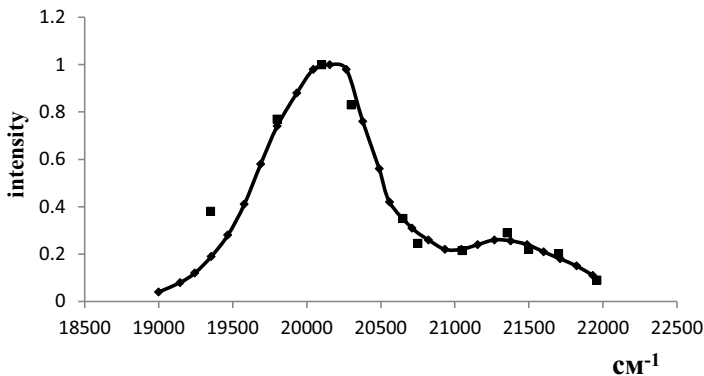for the CARS excitation profiles of the C–C stretching mode.

Both sets indicate that the major broadening mechanism is inhomogeneous ($\sigma \gg \Gamma$).

It should be mentioned that the non-compliance of the experimental results of the CARS excitation profile for the CH_3 band[5] with the theoretical curves appears because the band at ~1000 cm^{-1} overlaps with that of benzene at 992 cm^{-1} and, consequently, errors may accumulate during the computation of the CARS excitation profile.

The next effort in the numerical calculations was a joint minimization of the functional delta for the CARS excitation profiles of Ω_1 and Ω_2, which gave results that were in good agreement with experiment (Fig. 1).

The compliance obtained by joint minimization is a bit less exact than for individual minimization; however, if we compare the compliance by joint minimization to both compliances of individual minimization, then the joint minimization gives much more agreement with experimental data than the individual minimization of the functional. Also, one of the causes for a less exact compliance in joint minimization concludes in the limitation for the third active mode.

Comparing the results obtained in this work to the results for Stokes and anti-Stokes Raman excitation profiles of β-carotene, it can be noted that the dimensionless equilibrium shifts Q_0 are somewhat lower, and the broadening parameters Γ and σ are significantly lower in the presented work.

(a)
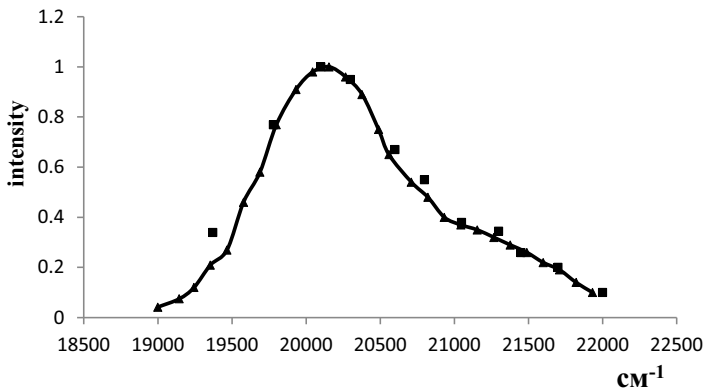
(b)

Fig. 1. CARS excitation profiles for the dominant active vibrations with frequencies $\Omega_1 = 1527\,\mathrm{cm}^{-1}$ (a), and $\Omega_2 = 1158\,\mathrm{cm}^{-1}$ (b). The circles are from the experiment.[5] The solid curves represent calculations from (4) with numerical values for the parameters specified from the set (13).

3. Conclusion

The basic model of vibronic interaction theory successfully used in investigations of anti-Stokes resonance Raman excitation profiles of π-conjugated systems has been applied to study the CARS excitation profiles of trans-β-carotene in benzene solution.

A complex quantitative analysis of the excitation profiles of β-carotene in benzene through the minimization of the mean square deviation of the theoretical curves from the experimental points was carried out.

Quantitative values of the theoretical parameters obtained because of the minimization are in good enough agreement with the theoretical parameters obtained by us for the resonance Raman excitation profiles.[6]

It was found that the major broadening mechanism is inhomogeneous, which coincides with the results obtained in our previous study[6] of the results from experiment[4] and contradicts the results obtained by others for the simple reason that before the introduction of the Voigt function, the band shape was assumed to be Lorentzian (homogeneous).

We hope that this paper will be a kind of impetus for experimenters to study a specific object under the same conditions (environment, temperature, etc.) with the mentioned nonlinear techniques because so far resonance Raman excitation profiles for β-carotene have been studied experimentally in various solvents but not in benzene.

ORCID

G. D. Tatishvili https://orcid.org/0009-0005-2000-0707
M. G. Zakaraya https://orcid.org/0009-0003-0514-4900
D. G. Gogoli https://orcid.org/0000-0003-0263-611X
S. P. Kruchinin https://orcid.org/0000-0002-0674-5826

References

1. M. D. Frank-Kamenetskij and A. V. Lukashin, *Usp. Fiz. Nauk* **116** (1975) 193.
2. M. Abramowitz and J. Stegun, *Handbook of Mathematical Functions* (Academic Press, New York, 1972).
3. M. G. Zakaraya and J. Ulstrup, *Opt. Commun.* **68** (1988) 107.
4. F. Inagaki and M. Tassumi, *J. Mol. Spectrosc.* **50** (1984) 286.
5. L. A. Carreira, T. C. Maguire and T. B. Malloy, *J. Chem. Phys.* **66** (1977) 2621.
6. M. G. Zakaraya, G. G. Maisuradze and G. D. Tatishvili, *Biofizika* **35** (1990) 906.
7. S. P. Kruchinin, R. I. Eglitis, S. P. Repetsky and I. G. Vyshyvana, *Crystals* **12**(2) (2022) 237.
8. S. P. Repetsky, I. G. Vyshyvana, S. P. Kruchinin and S. Bellucci, *Materials* **15** (2022) 739.